Abstract

This work presents a physics-infused reduced-order modeling (PIROM) framework towards the design, analysis, and optimization of ablating hypersonic thermal protection systems (TPS).

1 Introduction

At hypersonic speeds, aerospace vehicles experience extreme aero-thermal environments that requires specialized thermal protection systems (TPS) to shield internal sub-structures, electronics, and possibly crew members from the intense aerodynamic heating. The TPS is often composed of ablating materials – a high-temperature capable fibrous material injected with a resin that fills the pore network and strengthens the composite Amar2016. The TPS design promotes the exchange of mass through thermal and chemical reactions (i.e., pyrolisis), effectively mitigating heat transfer to the sub-structures.

As a result, accurate prediction for the ablating TPS response under extreme hypersonic heating becomes fundamental to ensuring survivability, performance, and safety of hypersonic vehicles. Not only is it necessary to assess the performance of the thermal management systems, but also the shape changes of the vehicle's outer surface induced by the ablating material, and its impact on the aerodynamics, structural integrity, and controllability. Unfortunately, high-fidelity simulations of ablating TPS remains a formidable challenge both theoretically and computationally.

On the theoretical side, the thermo-chemical reactions, coupled with the irregular pore network structure, translate into simplifying assumptions to reduce non-linearities, and make the resulting equations more amenable for engineering application and design analysis x. For instance, one of the most notable codes is the one-dimensional CMA code that was developed by Aerotherm Corporation in the 1960s Howard2015. Despite its practical use in...

Another example is the CHarring Ablator Response (CHAR) ablation code, which ignores elemental decompositions of the pyrolizing gases, assumes the gases to be a mixture of perfect gases in thermal equilibrium, and assumes no reaction or condensation with the porous network [**?**].

theoretically:

computationally:

2 Modeling of Ablating Thermal Protection Systems

This section presents the ablation problem for a non-decomposing TPS as a parametrized system of non-linear PDEs. These non-linear PDEs govern the energy of heat conduction and the pseudo-elastic material deformation of the mesh motion. Two different but mathematically-connected numerical solution strategies are provided: (1) a high-fidelity full-order model (FOM) based on a discontinuous Galerkin FEM, and (2) a thermo-elastic RPM based on a one-dimensional approximation to the energy and pseudo-elasticity equations.

2.1 Governing Equations

Consider a generic domain $\Omega \subset$, $d = 2$ or 3, illustrated in Fig. 1. A heat flux $q_b(x,t)$ is prescribed on the boundary Γ_q (i.e., Neumann boundary condition), and the temperature $T_b(x,t)$ is prescribed on boundary Γ_T (i.e., Dirichlet boundary condition), where $\Gamma_q \cup \Gamma_T = \partial\Omega$ and $\Gamma_q \cap \Gamma_T = \emptyset$. The ablation occurs only on the heated boundary Γ_q, and its effects are included into the energy equation using an Arbitrary Lagrangian-Eulerian (ALE) description. The ALE assumes that the displacement $\mathbf{w}(x,t) \in \mathbb{R}^d$ of the computational mesh moves with velocity $\mathbf{v}(x,t)$ that is different to the material velocity, which is fixed to zero in this work.

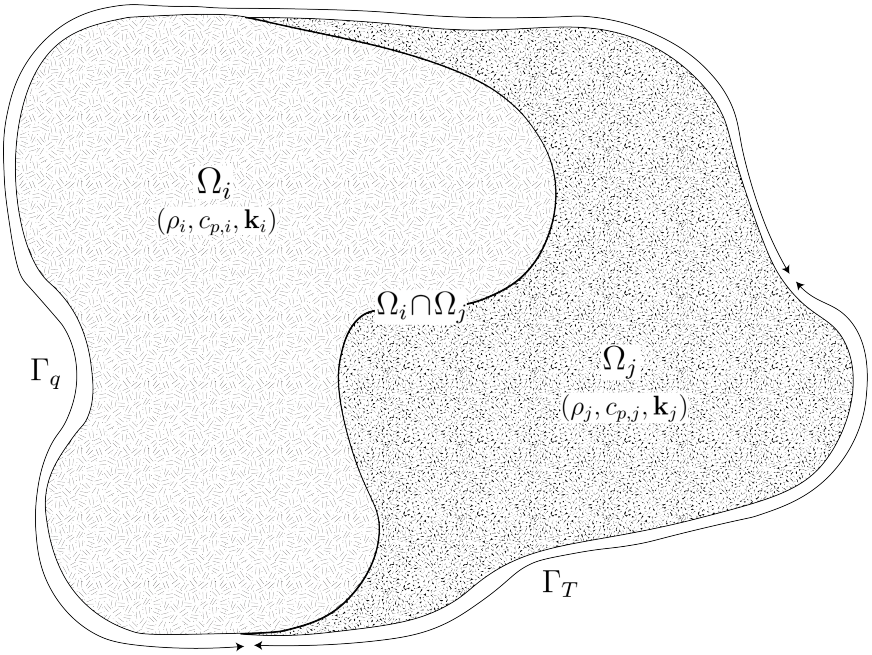

Figure 1: General domain Ω with prescribed heat flux $q_b(x,t)$ and temperature $T_b(x,t)$ on the boundaries Γ_q and Γ_T, respectively. The mesh moves with a velocity $\mathbf{v}(x,t)$, while the material velocity is $\mathbf{w}(x,t)$. draw mesh next to arbitrary domain with moving boundaries.

The transient heat conduction is described by the energy equation,

$$\rho c_p \left(\frac{\partial T}{\partial t} - \mathbf{v}(x,t) \cdot \nabla T \right) - \nabla \cdot (\mathbf{k} \nabla T) = \mathcal{Q}(x,t), \ x \in \Omega \tag{1a}$$

$$-\mathbf{k}\nabla T \cdot \mathbf{n} = q_b(x,t), \ x \in \Gamma_q \tag{1b}$$

$$T(x,t) = T_b(x,t), \ x \in \Gamma_T \tag{1c}$$

$$T(x,0) = T_0(x), \ x \in \Omega \tag{1d}$$

while the mesh motion is described by the pseudo-elasticity equation,

$$\nabla \cdot \boldsymbol{\sigma}(\mathbf{w}) = 0 \tag{2a}$$

$$\mathbf{w}(x,t) = \mathbf{w}_q(x,t), \quad x \in \Gamma_q \tag{2b}$$

$$\mathbf{w}(x,t) = 0, \quad x \notin \Gamma_q \tag{2c}$$

$$\mathbf{w}(x,0) = \mathbf{0} \tag{2d}$$

The density ρ, heat capacity c_p, and thermal conductivity $\mathbf{k} \in \mathbb{R}^{n_d \times n_d}$ are assumed to be constant with respect to temperature in this work. In the order they appear, the terms in eq. (1a) include, the unsteady energy storage, heat conduction, temperature advection due to mesh motion, and source terms due to boundary conditions.

The elasticity equation eq. (2a) states that the divergence of the stress tensor $\boldsymbol{\sigma}(\mathbf{w})$ is zero. The stress tensor is related to the strain tensor $\boldsymbol{\epsilon}(\mathbf{w})$ through Hooke's law,

$$\boldsymbol{\sigma}(\mathbf{w}) = \mathbb{D} : \boldsymbol{\epsilon}(\mathbf{w})$$

where $\mathbb{D}$ is the constitutive operator, ":" is the double contraction of tensors, and $\boldsymbol{\epsilon}$ is the symmetric strain tensor given by,

$$\boldsymbol{\epsilon}(\mathbf{w}) = \frac{1}{2} \left(\nabla \mathbf{w} + \nabla \mathbf{w}^T \right)$$

For instance, an isotropic material assumption results in,

$$\boldsymbol{\sigma} = \lambda \left(\nabla \cdot \mathbf{w}\right) \mathbf{I} + 2\mu \boldsymbol{\epsilon}(\mathbf{w})$$

where λ and μ are Lame constants that are arbitrarily selected to model the mesh motion. The "material" properties λ and μ can be chosen to tailor the mesh deformation and need not represent the actual material being modeled Amar2016.

The boundary conditions for the energy equation includes a heated surface (eq. (1b)) and a constant-temperature surface (eq. (1c)). The boundary conditions for the pseudo-elasticity equation are a function of the surface temperature $T_q(x,t)$ for $x \in \Gamma_q$ using a B' table. The B' table....

$$\mathbf{w}_q(x,t) = \int_0^t \mathbf{v}(x,\tau) d\tau = \int_0^t \mathbf{f}\left(T_q(x,\tau)\right) d\tau \tag{3}$$

2.2 Full-Order Model: Finite-Element Method

Consider a conforming mesh partition domain, where each element belongs to one and only one component. Denote the collection of all M elements as $\{E_i\}_{i=1}^M$. In an element E_i, its shared boundaries with another element E_j, Neumann BC, and Dirichlet BC are denoted as e_{ij}, e_{iq}, and e_{iT}, respectively. Lastly, $|e|$ denotes the length ($n_d = 2$) or area ($n_d = 3$) of a component boundary e.

For the i-th element, use a set of $n^{(i)}$ trial functions, such as polynomials, to represent the temperature distribution,

$$T^{(i)}(x,t) = \sum_{i=1}^{n^{(i)}} \phi_i^{(i)}(x) u_i^{(i)} \equiv \boldsymbol{\phi}^{(i)}(x)^T \mathbf{u}^{(i)}(t) \tag{4}$$

By standard variational processes, e.g., Cohen2018, the full governing equation is denoted as,

$$\mathbf{A}(\mathbf{u})\dot{\mathbf{u}} = \left(\mathbf{B}(\mathbf{u}) + \mathbf{C}(t,\mathbf{u})\right)\mathbf{u} + \mathbf{f}(t) \tag{5}$$

where $\mathbf{u} = \left[\mathbf{u}^{(1)}, \mathbf{u}^{(2)}, \ldots, \mathbf{u}^{(M)}\right]^T \in \mathbb{R}^{MP}$ includes all the DG variables, $\mathbf{f} \in \mathbb{R}^{MP}$ is the external forcing, and the system matrices $\mathbf{A}$, $\mathbf{B}$, and $\mathbf{C}$ are the matrices due to heat capacity, heat conduction, and temperature advection due to mesh motion, respectively. A detailed derivation of eq. (5) is provided in Appendix DG-FEM.

2.3 Reduced-Physics Model: Lumped-Capacitance Model

The lumped capacitance model (LCM) is a classical physics-based low-order model for predicting the temporal variation of average temeprature in multi connected components Incropera. The LCM is usually derived at the component level from a point of view of energy conservation. The following assumptions are employed: (1) in component (i) all variations of temperature with respect to space are ignored, and the temperature is described by a single uniform temperature $\bar{u}^{(i)}$; (2) between neighboring components (i) and (j) the heat flux is,

$$q_{ij} = \frac{\bar{u}^{(j)} - \bar{u}^{(i)}}{R_{ij}} \tag{6}$$

where R_{ij} is the thermal resistance. Empirically, for a component of istrisotropic heat conductivity k, length ℓ, and cross-section area A, the thermal resistance is $R = \ell/kA$. Between components i and j, define $R_{ij} = R_i + R_j$. In addition, the heat flux due to Dirichlet boundary condition is computed as $q_{iT} = (T_b - \bar{u}^{(i)})/R_i$.

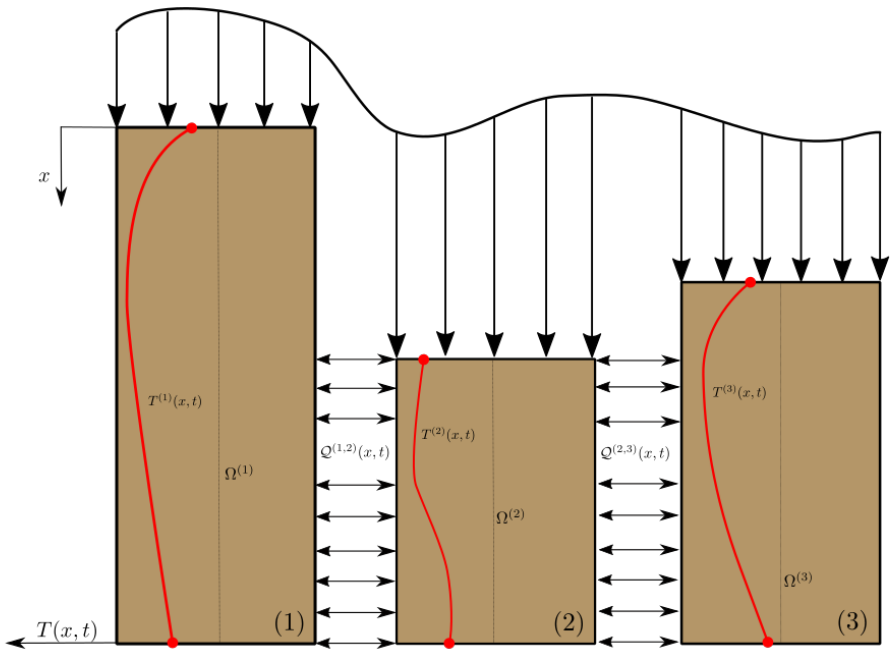

Figure 2: Partition of the TPS into three one-dimensional components.

At component i, the dynamics of LCM are given by,

$$\int_{E^{(i)}} \rho c_p \dot{\bar{u}}^{(i)} dE^{(i)} = \left(\sum_{j \in \mathcal{N}_i} \int_{e_{ij}} \frac{\bar{u}^{(j)} - \bar{u}^{(i)}}{R_{ij}} de_{ij} \right) + \int_{e_{iq}} q_b de_{iq} + \int_{e_{iT}} \frac{T_b - \bar{u}^{(i)}}{R_i} de_{iT} \tag{7a}$$

$$\bar{A}^{(i)} \dot{\bar{u}}^{(i)} = \left(\sum_{j \in \mathcal{N}_i} \frac{|e_{ij}|}{R_{ij}} \left(\bar{u}^{(j)} - \bar{u}^{(i)} \right) \right) + |e_{iq}| \bar{q}^{(i)} + \frac{|e_{iT}|}{R_i} \left(\bar{T}^{(i)} \right) \tag{7b}$$

note that there is no advection matrix since the temperature approximation requires space derivatives

2.3.1 Coarse Graining

Consider a DG model as in eq. (5) for M components and N elements; clearly $N \gg N$. Let $\mathcal{V}_j = \left\{ i | E^{(i)} \in \Omega^{(j)} \right\}$ be the indices of the elements belonging to the j-th component, so $E^{(i)} \in \Omega^{(j)}$ for $i \in \mathcal{V}_j$; number of elements in $\Omega^{(j)}$ is denoted as $|\mathcal{V}_j|$.

The ablation on the i-th component is modeled using a one-dimensional approximation to the temperature and mesh-motion equations in eq. (1d), and are given by,

$$\rho c_p \left(\frac{\partial T^{(i)}}{\partial t} - v^{(i)}(x,t) \frac{\partial T^{(i)}}{\partial x} \right) - \frac{\partial}{\partial x} \left(k \frac{\partial T^{(i)}}{\partial x} \right) - \mathcal{Q}^{(i)}_{\text{net}}(x,t) = 0 \tag{8a}$$

$$\frac{\partial}{\partial x} \left(\frac{\partial u^{(i)}}{\partial x} \right) = 0 \tag{8b}$$

with boundary conditions for the energy equation,

$$-k\frac{\partial T^{(i)}}{\partial x}\bigg|_{x=0} = q_b^{(i)}(t) \tag{9a}$$

$$-k\frac{\partial T^{(i)}}{\partial x}\bigg|_{x=\ell} = 0 \tag{9b}$$

and for the elasticity equation,

$$u^{(i)}(0,t) = \int_{t_0}^{t} v^{(i)}(\tau)d\tau = \int_{0}^{t} f(T_w^{(i)}(\tau))d\tau \tag{10a}$$

$$u^{(i)}(\ell,t) = 0 \tag{10b}$$

where $v^{(i)}(t)$ is the surface receding velocity due to ablation, which is a function of the surface temperature as in eq. (3). The surface velocity is computed from a cubic spline interpolate to a B' look-up table...

2.3.2 Thermal Solver

The FEM implementation details are supplied in Appendix x. For the n-th component, the result of the FEM discretization is a system of ODEs for the nodal temperatures, coupled to the neighboring component $n+1$ through the energy volumetric source term,

$$\mathbf{A}^{(i)}\frac{d\mathbf{T}^{(i)}}{dt} + \left(\mathbf{B}^{(i)} - \mathbf{C}^{(i)}(t)\right)\mathbf{T}^{(i)} = \mathbf{f}^{(i)}(t) \tag{11}$$

where,

- $\mathbf{A}^{(i)} \in \mathbb{R}^{M\times M}$ is the mass matrix,
- $\mathbf{B}^{(i)} \in \mathbb{R}^{M\times M}$ is the stiffness matrix,
- $\mathbf{C}^{(i)}(t) \in \mathbb{R}^{M\times M}$ is the advection matrix,,
- $\mathbf{T}^{(i)} \in \mathbb{R}^{M}$ is the vector of nodal temperatures, and
- $\mathbf{f}^{(i)}(t) \in \mathbb{R}^{M}$ is the input vector, which includes the Neumann boundary conditions and the net volumetric energy source term $\mathcal{Q}_{\text{net}}^{(i)}$.

where M is the number of nodes in the one-dimensional mesh for the i-th component.

2.3.3 Pseudo-Elastic Solver

Note that eq. (8b) is steady. Under the assumption that the mesh deformation is quasi-steady, it can be applied at each time step within an ablation simulation. For instance, a known value of the wall temperature $T_w(t)$ specifies a Dirichlet boundary condition for the displacement, and the resulting nodal displacements within the ablator are determined from eq. (2a).

Along the one-dimensional domain, the PDE in eq. (2a) simplifies to,

$$\frac{\partial^2 u^{(i)}}{\partial x^2} = 0 \tag{12}$$

which has the analytical solution,

$$u^{(i)}(x,t) = a(t)x + b(t) \tag{13}$$

Imposing the boundary conditions leads to,

$$u^{(i)}(x,t) = u^{(i)}(0,t)\left(\frac{x_1^{(i)} - x}{h^{(i)}}\right) \tag{14}$$

The mesh velocity is the time derivative of the displacement,

$$v^{(i)}(x,t) = \frac{\partial u^{(i)}(x,t)}{\partial t} = v^{(i)}(t)\left(\frac{x_1^{(i)} - x}{h^{(i)}}\right) \tag{15}$$

2.3.4 Coupling Scheme

2.3.5 Reduced-Physics Ablation Simulation

A Mathematical Details

A.1 Full-Order Model

To obtain the full-order numerical solution, the governing equation is spatially discretized using variational principles of Discontinuous Galerkin (DG) to result in a high-dimensional system of ordinary differential equations (ODEs). Furthermore, the DG model is written in an element-wise form, which is beneficial for subsequent derivations for the lower-order models. Note that the choice of DG approach here is mainly for theoretical convenience in the subsequent coarse-graining formulation. In the numerical results, the full-order TPS ablation simulations is computed using standard FEM instead, and the equivalence between DG and standard FEM is noted upon their convergence.

A.1.1 Domain Discretization

A.1.2 Weak Form of Discontinuous Galerkin Method

Choosing appropriate basis functions ϕ_k and ϕ_l and using the Interior Penalty Galerkin (IPG) scheme [**?**], the variational bilinear form for eq. (1a) is,

$$\sum_{i=1}^{M} a_{\epsilon,i}(\phi_k, \phi_l) = \sum_{i=1}^{m} L_i(\phi_k) \tag{16}$$

where ϵ is an user-specified parameter and,

$$a_{\epsilon,i}(\phi_k,\phi_l) = \int_{E^{(i)}} \left(\rho c_p \phi_k \frac{\partial \phi_l}{\partial t} + \nabla\phi_k \cdot (\mathbf{k}\nabla\phi_l) - \rho c_p \phi_k \mathbf{v}\cdot\nabla\phi_l\right) dE^{(i)} \tag{17a}$$

$$= -\sum_{j\in\mathcal{N}_i\cup\{T_b\}} \int_{e_{ij}} \{\mathbf{k}\nabla\phi_k\cdot n\}\,[\phi_l]\,de_{ij} + \epsilon \sum_{j\in\mathcal{N}_i\cup\{T_b\}} \int_{e_{ij}} \{\mathbf{k}\nabla\phi_l\cdot n\}\,[\phi_k]\,de_{ij}$$

$$+ \sigma \sum_{j\in\mathcal{N}_i\cup\{T_b\}} \int_{e_{ij}} [\phi_k]\,[\phi_l]\,de_{ij} \tag{17b}$$

$$L_i(v) = \epsilon \sum_{j\in\mathcal{N}_i\cup\{T_b\}} \int_{e_{ij}} (\mathbf{k}\nabla\phi_l\cdot n)\,T_b de_{ij} + \int_{e_{iq}} \phi_k q_b de_{iq} + \sigma\int_{e_{iT}} \phi_k T_b de_{iT} \tag{17c}$$

In the bi-linear form above, the notations [] and {} are respectively the jumps and averages at the boundary e_{ij} share by two elements E_i and E_j,

$$[u] = u\big|_{E_i} - u\big|_{E_j}, \quad \{u\} = \frac{1}{2}\left(u\big|_{E_i} + u\big|_{E_j}\right), \quad \text{for } x \in e_{ij} = E_i \cap E_j$$

Furthermore, in the bi-linear form, the terms associated with σ are introduced to enforce the Dirichlet boundary conditions; σ is a penalty factor whose value can depend on the size of an element. Depending on the choice of ϵ, the bi-linear form corresponds to symmetric IPG ($\epsilon = -1$), non-symmetric IPG ($\epsilon = 1$), and incomplete IPG ($\epsilon = 0$). All these schemes are consistent with the original PDE and have similar convergence rate with respect to mesh size. In the following derivations, the case $\epsilon = 0$ is chosen for the sake of simplicity.

A.1.3 Discontinuous Galerkin Model

Next, the DG-based model is written in an element-wise form. For the i-th element, use a set of P trial functions to represent the temperature as in eq. (4). Without loss of generality, the trial functions are assumed to be orthogonal, so that $\int_{E^{(i)}} \phi_k^{(i)}(x)\phi_l^{(i)}(x)dx = \left|E^{(i)}\right| \delta_{kl}$, where $\left|E^{(i)}\right|$ is the area ($n_d = 2$) or volume ($n_d = 3$) of the i-th element, and δ_{kl} is the Kronecker delta.

Using test functions same as trial functions, the dynamics $\mathbf{u}^{(i)}$ is obtained by evaluating the element-wise bi-linear forms,

$$a_{\epsilon,i}(\phi_k^{(i)}, T^{(i)}) = L_i(\phi_k^{(i)}), \quad k = 1, 2, \ldots, P \tag{18}$$

The above procedure yields,

$$\mathbf{A}^{(i)}\dot{\mathbf{u}}^{(i)} = \left(\mathbf{B}^{(i)} + \mathbf{C}^{(i)}(t)\right)\mathbf{u}^{(i)} + \sum_{j \in \mathcal{N}_i \cup \{T_b\}} \left(\mathbf{B}_{ij}^{(i)}\mathbf{u}^{(i)} + \mathbf{B}_{ij}^{(j)}\mathbf{u}^{(j)}\right) + \mathbf{f}^{(i)}(t) \tag{19}$$

where for $k, l = 1, 2, \ldots, P$,

$$\left[\mathbf{A}^{(i)}\right]_{kl} = \int_{E^{(i)}} \rho c_p \phi_k^{(i)} \phi_l^{(i)} dE^{(i)} \tag{20a}$$

$$\left[\mathbf{B}^{(i)}\right]_{kl} = \int_{E^{(i)}} \left(\nabla \phi_k^{(i)}\right) \cdot \left(\mathbf{k} \nabla \phi_l^{(i)}\right) dE^{(i)} \tag{20b}$$

$$\left[\mathbf{C}^{(i)}\right]_{kl} = \int_{E^{(i)}} \rho c_p \phi_k^{(i)} \mathbf{v} \cdot \nabla \phi_l^{(i)} dE^{(i)} \tag{20c}$$

$$\left[\mathbf{B}_{ij}^{(i)}\right] = \int_{e_{ij}} -\left\{\mathbf{k}\nabla\phi_k^{(i)} \cdot \hat{n}\right\} \phi_l^{(i)} + \sigma \left[\phi_k^{(i)}\right] \phi_l^{(i)} de_{ij} \tag{20d}$$

$$\left[\mathbf{B}_{ij}^{(j)}\right] = \int_{e_{ij}} \left\{\mathbf{k}\nabla\phi_k^{(i)} \cdot \hat{n}\right\} \phi_l^{(j)} - \sigma \left[\phi_k^{(i)}\right] \phi_l^{(j)} de_{ij} \tag{20e}$$

$$\left[\mathbf{f}^{(i)}\right]_k = \int_{e_{iq}} \phi_k^{(i)} q_b de_{iq} + \sigma \int_{e_{iT}} \phi_k^{(i)} de_{iT} \tag{20f}$$

Note that the matrices $\mathbf{A}^{(i)}$, $\mathbf{C}^{(i)}$, and $\mathbf{B}_{ij}$ depend on ρ, c_p, and $\mathbf{k}$, respectively, and hence can be a non-linear function of $\mathbf{u}$. Since the trial functions are orthogonal, if ρc_p is constant within an element, $\mathbf{A}^{(i)}$ is diagonal; otherwise, $\mathbf{A}_i$ is symmetric and positive definite as $\rho c_p > 0$.

For compactness, the element-wise model in eq. (19) is also written in matrix form,

$$\mathbf{A}(\dot{\mathbf{u}}) = (\mathbf{B}(\mathbf{u}) + \mathbf{C}(t, \mathbf{u}))\,\mathbf{u} + \mathbf{f}(t) \tag{21}$$

where $\mathbf{u} = \left[\mathbf{u}^{(1)}, \mathbf{u}^{(2)}, \cdots, \mathbf{u}^{(M)}\right]^T \in \mathbb{R}^{MP}$ includes all DG variables, $\mathbf{f} = \left[\mathbf{f}^{(1)}, \mathbf{f}^{(2)}, \ldots, \mathbf{f}^{(M)}\right]^T \in \mathbb{R}^{MP}$, $\mathbf{A}$ and $\mathbf{C}$ are matrices of M diagonal blocks whose i-th blocks are $\mathbf{A}^{(i)}$ and $\mathbf{C}^{(i)}$, and $\mathbf{B}$ is a matrix of $M \times M$ blocks whose (i, j)-th block is,

$$\mathbf{B}_{ij} = \begin{cases} \mathbf{B}^{(i)} + \sum_{j \in \mathcal{N}_i \cup \{T_b\}} \mathbf{B}_{ij}^{(i)}, & i = j \\ \mathbf{B}_{ij}^{(j)}, & i \neq j \end{cases} \tag{22}$$

The dependency of $\mathbf{A}$, $\mathbf{B}$, and $\mathbf{C}$ on $\mathbf{u}$ is explicitly noted in eq. (21), which is the source of non-linearity in the current TPS problem. Moreover, the mesh velocity $\mathbf{v}$ varies with space and time, and thus the advection matrix $\mathbf{C}$ varies with time as a function of q_b.